PNAS Nexus, 2025, 4, pgae563
https://doi.org/10.1093/pnasnexus/pgae563
Advance access publication 17 December 2024
Research Report

Sustainable production of 2,5-diformylfuran via peroxymonosulfate-triggered mild catalytic oxidation of lignocellulosic biomass

Ke-Yu Chen[a,b], Lin-Qian Yu[a,b], Yun-Xin Huang[a,b], Wu-Jun Liu[c], Bao-Cheng Huang[a,b,*], Ren-Cun Jin[a,b] and Han-Qing Yu[c,*]

[a]School of Engineering, Hangzhou Normal University, Hangzhou 310018, China
[b]School of Life and Environmental Sciences, Hangzhou Normal University, Hangzhou 310018, China
[c]CAS Key Laboratory of Urban Pollutant Conversion, Department of Environmental Science and Engineering, University of Science and Technology of China, Hefei 230026, China
*To whom correspondence should be addressed: Email: huangbc@hznu.edu.cn (B.-C.H.); Email: hqyu@ustc.edu.cn (H.-Q.Y.)
Edited By Yi-Jun Xu

Abstract

The relentless depletion of fossil fuels accentuates the urgent necessity for the sustainable synthesis of chemicals from renewable biomass. 5-Hydroxymethylfurfural (HMF), extracted from lignocellulosic biomass, emerges as a beacon of hope for conversion into value-added chemicals. However, the inherent susceptibility of its unsaturated aldehyde groups to excessive oxidation often culminates in undesired reactions, compromising both the yield and specificity of the desired products. Here, we introduce a holistic methodology for the cost-effective and ecologically responsible generation of 2,5-diformylfuran (DFF), through the heterogeneously catalyzed oxidation of HMF utilizing peroxymonosulfate (PMS) under benign conditions. This strategy, characterized by the meticulous enhancement of surface ketone groups via a mixed-salt-assisted co-pyrolysis technique, achieves an unparalleled selective activation of PMS, engendering singlet oxygen to catalyze the oxidation of HMF into DFF with a selectivity surpassing 80%. Life-cycle assessments underscore a negligible impact on human health, ecosystems, and natural resources, endorsing the holistic utilization of biomass. This integration of pyrolysis for the creation of functional carbonaceous materials within biomass conversion processes significantly enhances sustainability and economic viability, while paving green pathways for selective biomass oxidation and the production of high-value chemicals.

Keywords: singlet oxygen, biomass upgrading, 2,5-diformylfuran, ketone, selective oxidation

Significance Statement

Valorizing lignocellulosic biomass for chemicals production is pivotal in advancing green chemistry practice. A biomass refining process centered on the platform compound of 5-hydroxymethylfurfural (HMF) is a viable route for value-added chemical production. However, the precise control of HMF oxidation and the selective synthesis of target products under environmentally benign conditions remains as the bottleneck for biomass-to-chemical conversion. This study fabricates the ketone-rich biochar, which catalyzes peroxymonosulfate cleavage to achieve a 100% singlet oxygen generation and thereby selectively oxidizes HMF to 2,5-diformylfuran under mild reaction conditions. Consequently, a fine chemical production process, which is economically viable and environmentally sustainable, from lignocellulosic biomass is built up. This work represents a significant advancement in the green production of chemicals by utilizing biomass resource.

Introduction

The production of chemicals, heavily reliant on petrochemical feedstocks, confronts formidable challenges due to its substantial emissions, exacerbating climate change and environmental degradation (1). This issue is further exacerbated by the growing demands in sectors such as food production and health care, amplifying existing environmental concerns (2). Thus, there emerges an imperative for sustainable and eco-friendly chemical synthesis, distinguished by reduced carbon emissions via the adoption of renewable resources (3, 4). Lignocellulosic biomass, in this context, presents a promising avenue for the sustainable production of biofuels and biochemicals, capturing significant attention over recent years (5–7). Within this framework, 2,5-diformylfuran (DFF) is identified as a crucial precursor for myriad downstream applications, including the manufacturing of fine chemicals, pharmaceuticals, sterilizing agents, and

Competing Interest: The authors declare no competing interests.
Received: September 6, 2024. **Accepted:** December 1, 2024

functional polymers (8–10). The conversion process involves the hydrolysis of cellulose or hemicellulose to produce the platform compound 5-hydroxymethylfurfural (HMF), followed by its subsequent oxidative treatment (8, 11). Conventionally, this oxidation process utilizes oxygen under stringent conditions to generate reactive species capable of converting HMF to DFF (9, 12, 13). However, the severe reaction conditions and the inherent compromise between conversion efficiency and product selectivity greatly limit the practical application of this methodology. Furthermore, the natural reactivity of HMF's unsaturated aldehyde groups frequently results in its over-oxidation, diminishing DFF yields (14). Therefore, the strategic selection of oxidation species with moderate oxidation capacities, coupled with the execution of the reaction under milder conditions to minimize energy consumption, is identified as a critical strategy for the sustainable production of DFF.

In stark contrast to ephemeral and indiscriminate radicals (15), metastable singlet oxygen ($^1O_2$) exhibits a moderate redox potential among reactive oxygen species and demonstrates exceptional selectivity toward electron-rich organics (16), establishing itself as the ideal oxidant to circumvent the over-oxidation challenge in DFF production from HMF (17). In addition to activating O_2 molecules via photosensitization, the catalysis of peroxymonosulfate (PMS) cleavage through ketone structures also presents an effective means of generating $^1O_2$ (18, 19). By exploiting the oxygen-rich nature of biomass, the direct synthesis of ketone-enriched biochar from biomass waste not only facilitates the generation of $^1O_2$ from PMS, but also mitigates the environmental footprint and enhances process economics.

Here, we propose an innovative strategy for the selective oxidation of HMF under mild conditions, leveraging the generation of $^1O_2$ via the catalytic cleavage of PMS. Initially, we utilized a mixed-salt-assisted co-pyrolysis approach to customize the surface oxygen functionalities of biochar, employing representative biomass as precursors, and successfully synthesized a ketone-enriched biochar catalyst (KBC). Subsequently, the production of DFF from HMF via biochar-catalyzed PMS decomposition under mild conditions (neutral pH, ambient pressure, and aqueous solvent) was experimentally investigated, with a comprehensive elucidation of the underlying reaction mechanism. Finally, an economic evaluation and life-cycle assessment (LCA) of the process were performed. In this way, a green and sustainable process for biomass-to-DFF production, characterized by high yield and selectivity, was successfully established.

Results and discussion

Enriching ketone structure on biochar surface via mixed-salt-assisted pyrolysis

Through the application of mixed salts consisting of $ZnCl_2$ and KCl, the surface oxygen functionalities of biomass precursors were refined in the pyrolysis process (Fig. S1), leading to the creation of the KBC. X-ray diffraction (XRD) patterns and X-ray photoelectron spectroscopy (XPS) surveys conclusively verified the absence of metallic contaminants in the resulting biochar (Figs. S2 and S3). High-resolution O 1s XPS spectra of the KBC were subjected to curve fitting, revealing three distinct peaks (Fig. 1a), i.e. C=O (~531.2 eV), O=C–O (~532.4 eV), and C–O (~533.7 eV) (20). Mixed salt dosage largely affected the relative abundances of these oxygen functionalities. Particularly, a 2:1 ratio of mixed salts to precursor facilitated the highest oxygen incorporation, with the biochar labeled as KBC-2, showcasing an oxygen content of 21.70 wt.% (Fig. S4) and C=O groups representing nearly 45% of this composition (Table S1). Conversely, the direct pyrolysis of biomass without salt incorporation (referred to as BC) resulted in a significantly lower oxygen content of 9.88 wt.%. The strategic addition of $ZnCl_2$/KCl amplified the overall oxygen content but also elevated the C=O group ratio within the catalyst.

To elucidate the potential role of $ZnCl_2$/KCl in ketone structure formation, a suite of pyrolysis products prepared at varying temperatures (200–800 °C) with a constant salt dosage ratio of 2:1 were analyzed via Fourier transform infrared spectroscopy (FTIR) (Fig. 1b). Products carbonized at temperatures ranging from 200 to 600 °C exhibited characteristic stretching vibrations of C=C aromatic ring (1,600 cm^{-1}) and –COOH (1,700 cm^{-1}). After increasing the temperature to 700 °C, a discernible stretching vibration of C=O at 1,650 cm^{-1} emerged, supplanting the previous peaks. In contrast, the FTIR spectrum of biochar catalyst prepared without mixed salt displayed no conspicuous C=O peak until 800 °C (Fig. S5). This result suggests that the $ZnCl_2$/KCl initially facilitated dehydration to engender a short-chain structure during pyrolysis, followed by cross-linking and cyclization to construct the carbon framework, culminating in the induction of additional C=O bonds owing to the presence of Lewis acid $ZnCl_2$ (21).

The structural properties of KBC-2, distinguished by its highest ketone group content, were further characterized. Scanning electron microscopy (SEM) images reveal that KBC-2 exhibited a markedly irregular and interconnected porous structure, as opposed to the smooth surface of the BC (Fig. 1c). N_2 adsorption–desorption isotherms corroborated this observation (Fig. S6), highlighting the formation of meso- and microporous structures, attributed to the catalytic templating effect of mixed salts (22). Such morphological and structural characteristics (Fig. S7) enhanced the material's reactive site accessibility, thereby potentially improving reaction kinetics for heterogeneous catalysis. Thermogravimetric analysis (TGA) and differential scanning calorimetry (DSC) underscored a complete weight loss of the precursor at 700 °C, revealing the protective efficacy of the mixed salt (Fig. 1d and e), which transitioned to a liquid phase at 256 °C, serving as a barrier during pyrolysis. This protective action likely preserved the feedstock from rapid decomposition (23, 24), thereby optimizing material yield with increased salt proportions (Fig. 1f).

Expanding this mixed salt incorporation strategy to other biomass varieties demonstrated a consistent increase in surface ketone functionalities, highlighting the method's efficacy across diverse biomass types (Table S2). A comparative analysis with carbon materials from prior studies reveals that KBC-2 boasted a superior ketone group presence (Table S3), underscoring the potent impact of $ZnCl_2$/KCl addition in augmenting the ketone content of biomass-derived materials, thereby enhancing their utility in sustainable chemical synthesis applications.

Selective oxidation of HMF into DFF by catalyzing PMS cleavage

The deployment of KBC for catalyzing the cleavage of PMS and HMF conversion was evaluated under mild reaction conditions. HMF, containing two distinct reactive functional groups, has the potential to oxidize and yield four furan derivatives, including the coveted DFF, among others (Fig. 2a). In trials devoid of any catalyst, a mere 4.5% conversion of HMF was observed via spontaneous PMS decomposition, without any formation of DFF. The introduction of BC slightly improved the conversion rate to 9.4%, yet failed to foster any significant accumulation of DFF. A series of catalysts, developed under varying mixed salt-to-precursor

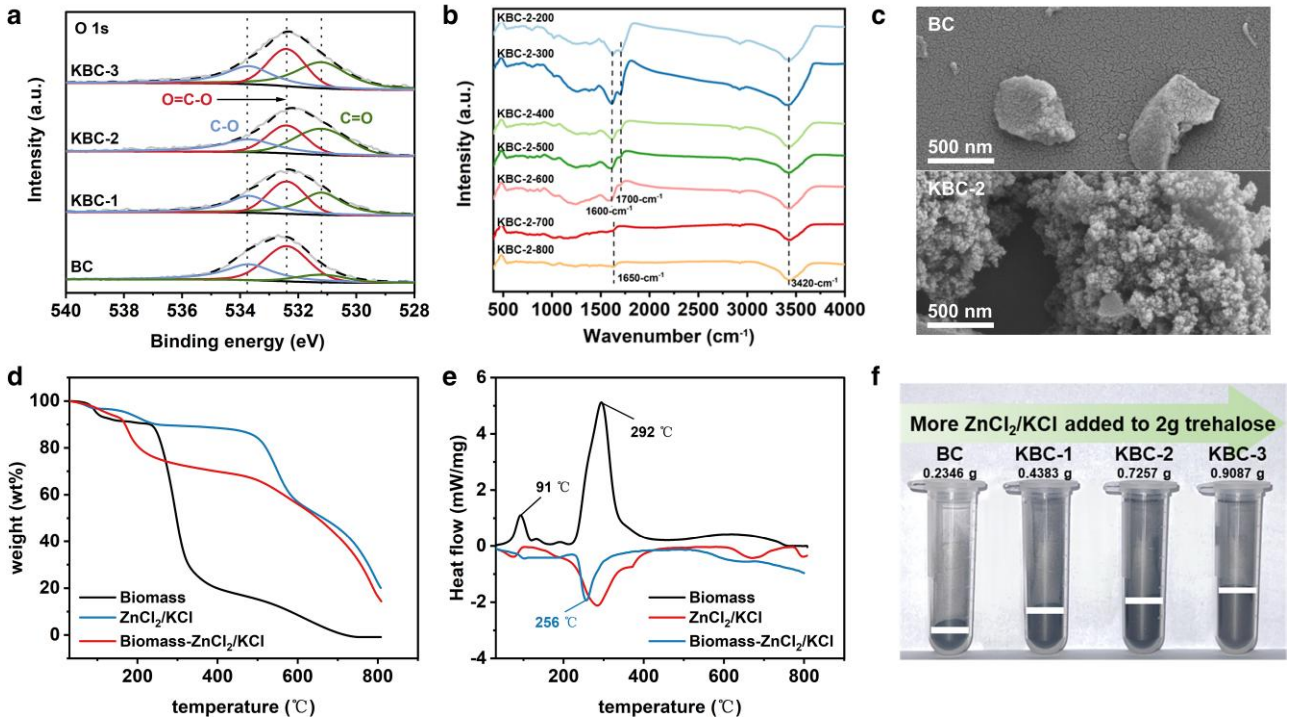

Fig. 1. Synthesis and characterizations of catalysts. a) High-resolution O 1s XPS spectra of BC, KBC-1, KBC-2, and KBC-3. b) FTIR spectra of biochar carbonized at different temperatures ranging from 200 to 800 °C under the mixed salt mass ratio of 2:1. c) SEM images of BC and KBC-2. d) TG and e) DSC diagrams of precursor, mixed salt, and the precursor/salt mixture. f) Photographs of BC, KBC-1, KBC-2, and KBC-3.

ratios (1:1 for KBC-1, 2:1 for KBC-2, and 3:1 for KBC-3), demonstrated a substantial impact on the selective oxidation of HMF (Figs. 2b and S8–S10). Remarkably, KBC-2 outperformed its counterparts by achieving an HMF conversion rate of 96.7%, with a DFF yield of 69.8% and selectivity exceeding 82%, under optimal conditions (Fig. 2c). This setup showcased numerous advantages, including operational mildness, heightened efficiency, exceptional selectivity, and minimal necessity for solvent post-treatment, establishing it as an unparalleled method for HMF-to-DFF conversion to date (Fig. 2d and Table S4). Further investigation into the stability of KBC-2 through recycling experiments indicated a minor decline in activity over successive uses, and annealing was found to restore its original catalytic vigor (Fig. S11). Post-use analysis indicated the maintenance of the C=O functional group content in KBC-2, while the surface C–O content increased, potentially explaining the slight dip in catalytic efficiency.

In light of these findings, the mechanism of HMF oxidation mediated by the KBC-2/PMS system was further investigated and in situ Raman spectroscopy was employed to analyze the evolution of HMF in solution (Fig. 2e). The solution spectra encompassing HMF, DFF, and assorted by-products along with the band distributions of their principal functional groups are presented in Fig. S12. Along with the oxidation of HMF (Fig. 2f), the C–O band of the methylol group appeared stably at 1,030 cm^{-1}, while the C–H band was redshifted to 1,356 cm^{-1}. This observation suggests oxidative species' interaction with the C–H bond of methylol groups as the initial oxidation step. Over time, a decrease in methylol group peaks (1,030 and 1,367 cm^{-1}) and an increase in formyl group peaks (1,668 and 1,400 cm^{-1}) indicated a preferential transformation from alcohols to aldehydes, signifying DFF formation. Moreover, the characteristic peak at 1,668 cm^{-1}, associated with the formyl group, redshifted to 1,672 cm^{-1}, suggesting the potential formation of 5-formyl-2-furancarboxylic acid among the by-products, owing to minimal HMF adsorption onto the catalyst. This conjecture was further supported by minor fluctuations observed in the peak at 1,352 cm^{-1}, indicative of HMF's limited affinity for the material surface. Therefore, the oxidative species bind to the C–H bond of the methylol group and oxidize it to form the formyl group through dehydrogenation, which was the main contribution to the selective oxidation of HMF to DFF.

To investigate the rate-determining step in formyl group formation (25), kinetic isotope effects (KIEs) were investigated using deuterated HMF molecules (R-CH_2OD and R-CD_2OH) (Fig. S13). As depicted in Fig. 2g and h, the KIE, defined as the ratio of oxidation rates for un-deuterated and deuterated HMF, was assessed. For R-CH_2OD, the KIE value was determined to be 1.35, which was consistent with a secondary KIE and implied a smaller difference in reaction activation energies throughout the reaction trajectory. In contrast, R-CD_2OH showed a notably higher KIE value of 6.59, which was much greater than unity and consistent with a primary KIE whereby the chemical bond involving the isotope was broken during the rate-determining step of the overall reaction. In conclusion, these findings indicate that the activation of C–H bonds within hydroxymethyl groups on HMF molecules by $^1O_2$ involved kinetically relevant steps in the oxidation of HMF to DFF.

Key role of $^1O_2$ in the selective oxidation of HMF into DFF

The application of KBC-2 as a catalyst to activate PMS and facilitate the selective oxidation of HMF to DFF was examined, emphasizing the creation of $^1O_2$ as the primary oxidative species. Previous studies have shown the dual potential of PMS activation by carbon-based catalysts to produce either radical or nonradical species. In our work, the specific preparation of KBC-2 aimed at

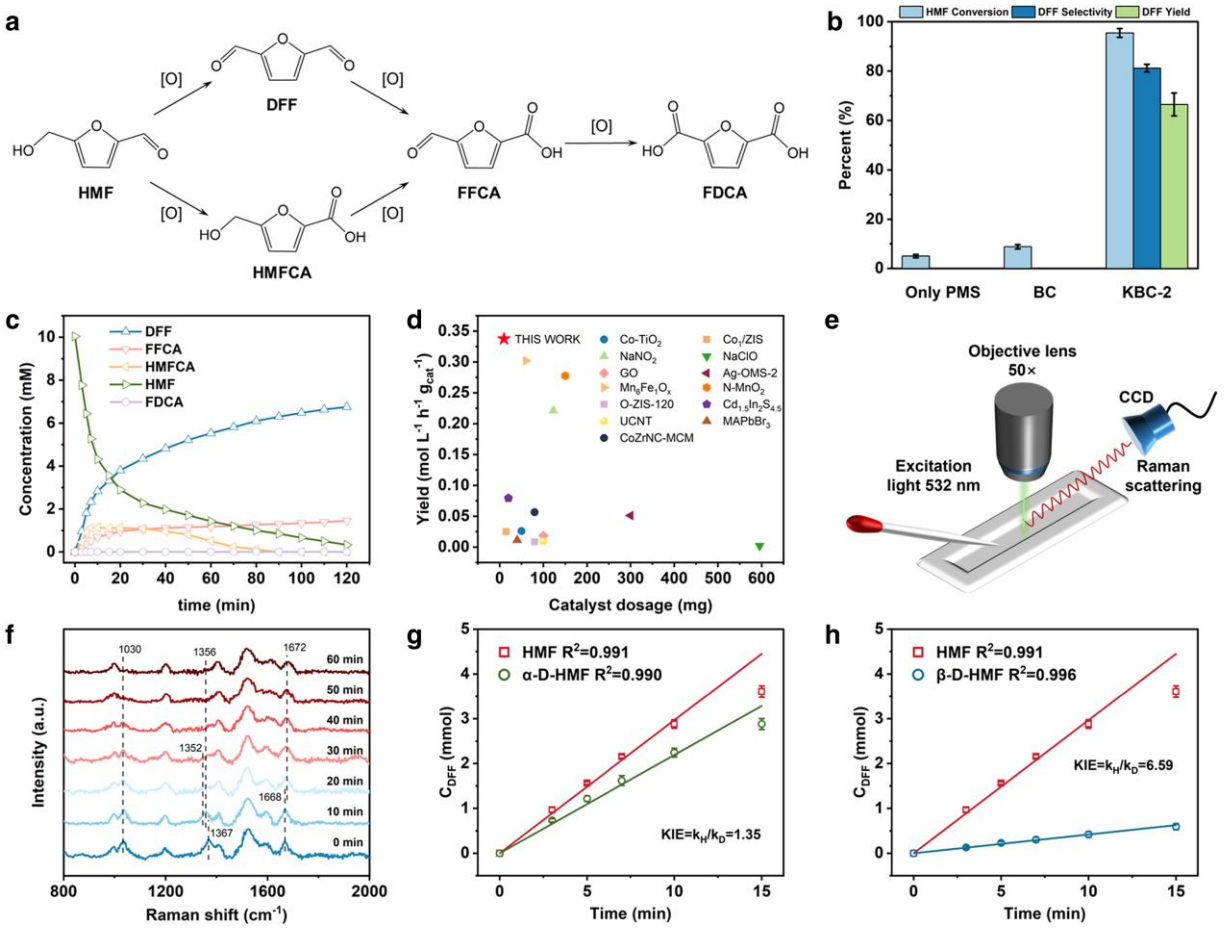

Fig. 2. Selective oxidation of HMF to DFF. a) Schematic illustration of the potential oxidation products from HMF. b) Performance of various catalysts for the selective oxidation of HMF to DFF. Reaction conditions: 5 mg of catalyst, 10 mM HMF, 20 mM PMS, 5 mL of water, 2 h, 50 °C. c) Concentrations versus time plot of HMF, DFF, and other products at various times. d) Comparison of the normalized kinetics of the selective oxidation of HMF to DFF using KBC-2 in this study and in the literature (details in Table S4). e) Schematic illustration of the in situ Raman test. f) In situ Raman spectra of a 10-mM HMF solution recorded with the KBC-2/PMS system. KIEs of KBC-2 catalysis of g) α-D-HMF and h) β-D-HMF.

generating exclusively $^1O_2$, as evidenced by minimal influence of alcohols on HMF conversion (Fig. 3a), suggesting the negligible role of radicals in the oxidation process (26, 27). The addition of potassium dichromate, effective in scavenging unbound electrons (28), did not greatly alter oxidation outcomes (Fig. 3a), further negating the possibility of electron transfer mechanism (Fig. S14). Conversely, the introduction of furfural (FFA) markedly reduced the efficiency of HMF oxidation, corroborating the exclusive generation of $^1O_2$. The generation of $^1O_2$ in the KBC-2/PMS system was also confirmed by using 1,3-diphenylisobenzofuran as a selective probe (Fig. S15). Electron paramagnetic resonance (EPR) analysis, employing 2,2,6,6-tetramethylpiperidine (TEMP) and 5,5-dimethyl-1-pyrroline N-oxide (DMPO) as traps for $^1O_2$ and radicals, respectively (29, 30), displayed a distinct TEMP-$^1O_2$ signal in the KBC-2/PMS system, confirming $^1O_2$'s predominance (Figs. 3b and S16). Notably, the intensity of $^1O_2$ signal followed the order KBC-2 > KBC-1 > KBC-3, indicating that an increased abundance of ketone groups enhanced $^1O_2$ yield.

In situ Raman spectroscopy provided insights into the surface bonding reaction between the catalyst and PMS, validating the $^1O_2$ production pathway. As shown in Figs. 3c and S17, the characteristic peaks at 1,060, 982, and 884 cm^{-1} were attributed to HSO5–, SO_4^{2-}, and O–O in PMS, respectively (31). After adding KBC-2, a significant decrease in the intensity of the HSO_5^- peak at 1,060 cm^{-1} was observed, while the peak attributed to SO_4^{2-} was redshifted to 986 cm^{-1}. A new peak near 838 cm^{-1} emerged, which was attributed to the extended bending vibration of the peroxide bond in the combined state PMS* (32). As the reaction progressed, the distinctive O–O bond and HSO_5^-peaks gradually disappeared, while the intensity of the SO_4^{2-} peak steadily increased, thus affirming that the active site on KBC-2 favored the $^1O_2$ generation through O–O bond cleavage after binding to the S=O bond in PMS.

To verify the role of ketone groups on $^1O_2$ evolution, we endeavored to neutralize the oxygen functional groups of KBC-2 utilizing various masking agents. Following the Boehm titration principle (33), we designated the treated samples as KBC-2–C_2H_5ONa and KBC-2–NaOH, where C_2H_5ONa reacted with oxygen-containing functional groups encompassing carbonyl groups, while NaOH reacted with groups distinct from carbonyl groups. Additionally, the KBC-2–phenylhydrazine (PH) catalyst was prepared using PH to selectively target the elimination of the C=O functional group (Fig. S18) (34). From the XPS spectra (Fig. S19) combined with organic elemental analysis, it was found that the C_2H_5ONa-treated catalyst was devoid of any oxygen functional groups, while the PH-treated counterparts lacked C=O, and the NaOH-treated catalyst predominantly contained C=O, as anticipate. Subsequent HMF oxidation utilizing treated catalysts

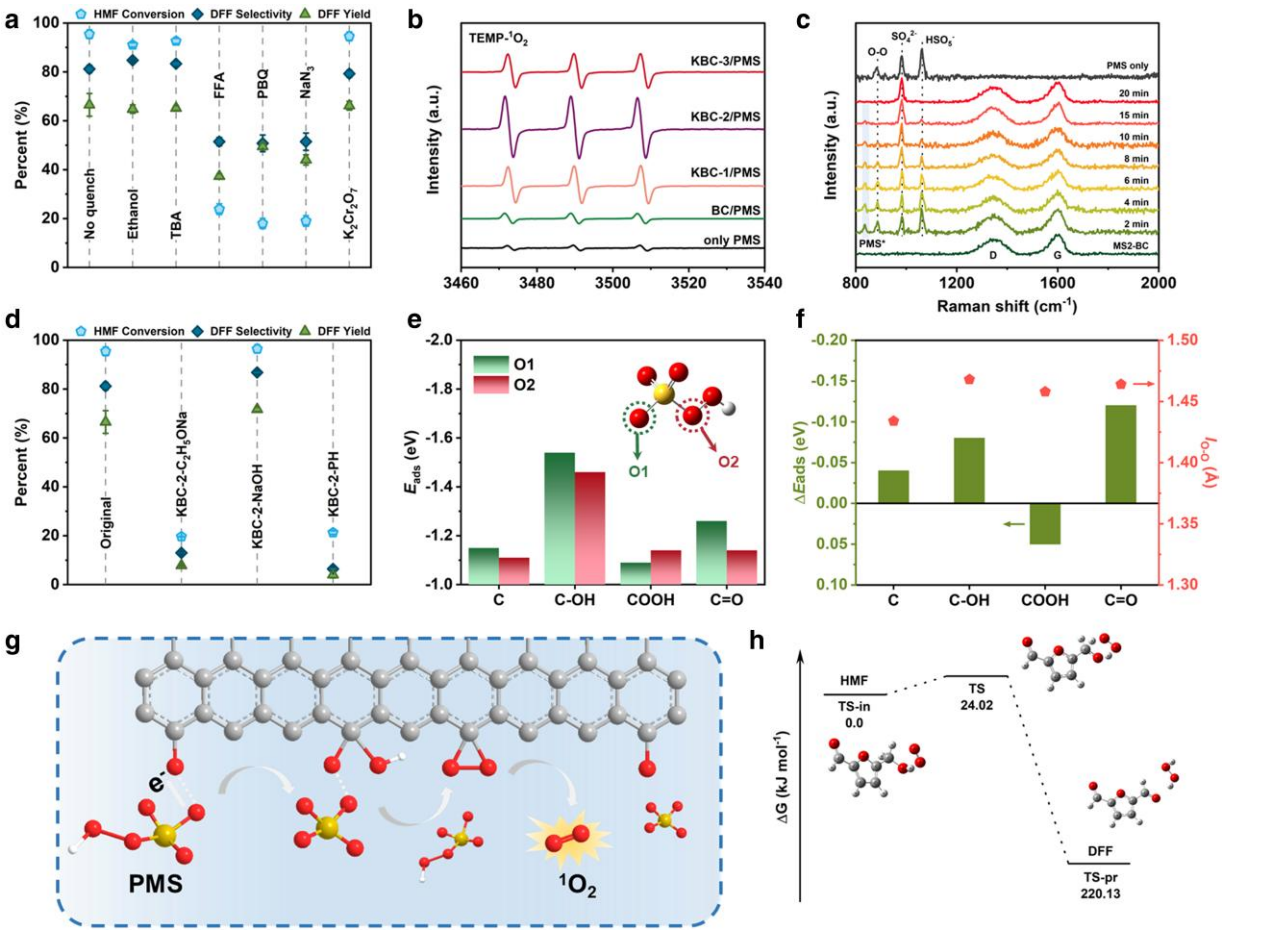

Fig. 3. Mechanism of selective oxidation. a) Performance of selective oxidation of HMF to DFF under different quenching conditions. b) EPR spectra of BC-, KBC-1-, KBC-2-, and KBC-3-catalyzed PMS activation in the presence of TEMP. c) In situ Raman spectra of the KBC-2/PMS system. d) Selective oxidation of HMF to DFF by KBC-2 treated with different alkaline reagents. Reaction conditions: 5 mg of catalyst, 10 mM HMF, 20 mM PMS, 5 mL of water, 2 h, 50 °C, 20 mM quencher. e) Calculated absorption energy for the different absorption configurations (O1 and O2). f) Different ΔE_{ads} and O–O bond lengths for two adsorption configurations (O1 and O2). g) Possible mechanism for the generation of $^1O_2$ from the reaction between C=O and PMS on the catalyst surface. h) Energy barrier diagram for H-atom abstraction of HMF by $^1O_2$.

(Fig. 3d) showcased a decline in HMF conversion to 19.7% by KBC-2–C_2H_5ONa, while the HMF conversion by KBC-2–NaOH remained almost unchanged compared with that of the original material and the DFF selectivity increased to 86.3%. The HMF conversion efficiency by KBC-2–PH was similar to that of KBC-2–C_2H_5ONa, but the selectivity and yield of DFF were lower. It was observed that KBC-2–PH facilitated the detection of the characteristic ·OH peak, attributed to the activation effect of other oxygen-containing functional groups on the catalyst's surface (Fig. S20). In contrast, the $^1O_2$ signal in KBC-2–NaOH/PMS system was notably intensified compared with the pristine material (35). These observations strongly imply that the ketone structure on the KBC-2 surface effectively governed the PMS activation process, preventing the generation of radicals from other oxygen-containing functional groups and endowing the catalyst's ability to 100% generate $^1O_2$.

In general, oxidative species generation is determined by the selective adsorption of O atoms within the PMS molecule onto the catalyst surface (Fig. 3e). Catalytic site combining with O2 site may promote O–O bond breaking and the formation of ·OH and $SO_4^{\cdot-}$, whereas catalyst binding with O1 site may induce H atom loss or the generation of $^1O_2$ through O–O bond rupture (36). Utilizing density functional theory (DFT) calculations, we explored the correlation between the type of oxygen functional groups at the catalyst edge and the selectivity of oxidative species generation from activated PMS. Previous works have shown that the difference in adsorption energy between adsorption configurations ($\Delta E_{ads} = E_{ads\text{-}O1} - E_{ads\text{-}O2}$) is positively correlated with the selectivity for $^1O_2$ generation, rendering ΔE_{ads} a descriptor for discerning selective $^1O_2$ generation (37, 38). The structure was optimized to obtain the lowest energy configuration of the possible adsorption types of PMS molecules on various oxygen-containing functional groups (Fig. S21). As shown in Fig. 3e and f, the C=O site exhibited a greater difference in ΔE_{ads} compared with other oxygen-containing functional groups. Specifically, C=O preferentially adsorbed on the O1 site, thereby promoting the activation and decomposition of PMS to generate $^1O_2$ by stretching the O–O bond (Fig. 3g).

To gain further insight into the mechanism of HMF oxidation to DFF using $^1O_2$, we conducted DFT calculations of the electrostatic potential mapping and Fukui index of the HMF molecule (Figs. S22 and S23) (39, 40). The electrostatic potential plot revealed the electron-rich nature of the HMF hydroxymethyl group, while the Fukui index identified the reactive sites that were susceptible to electrophilic attack, specifically the C10 and O13 sites within the hydroxymethyl group. Subsequent intrinsic reaction coordinate and energy barrier calculations elucidated the thermodynamic

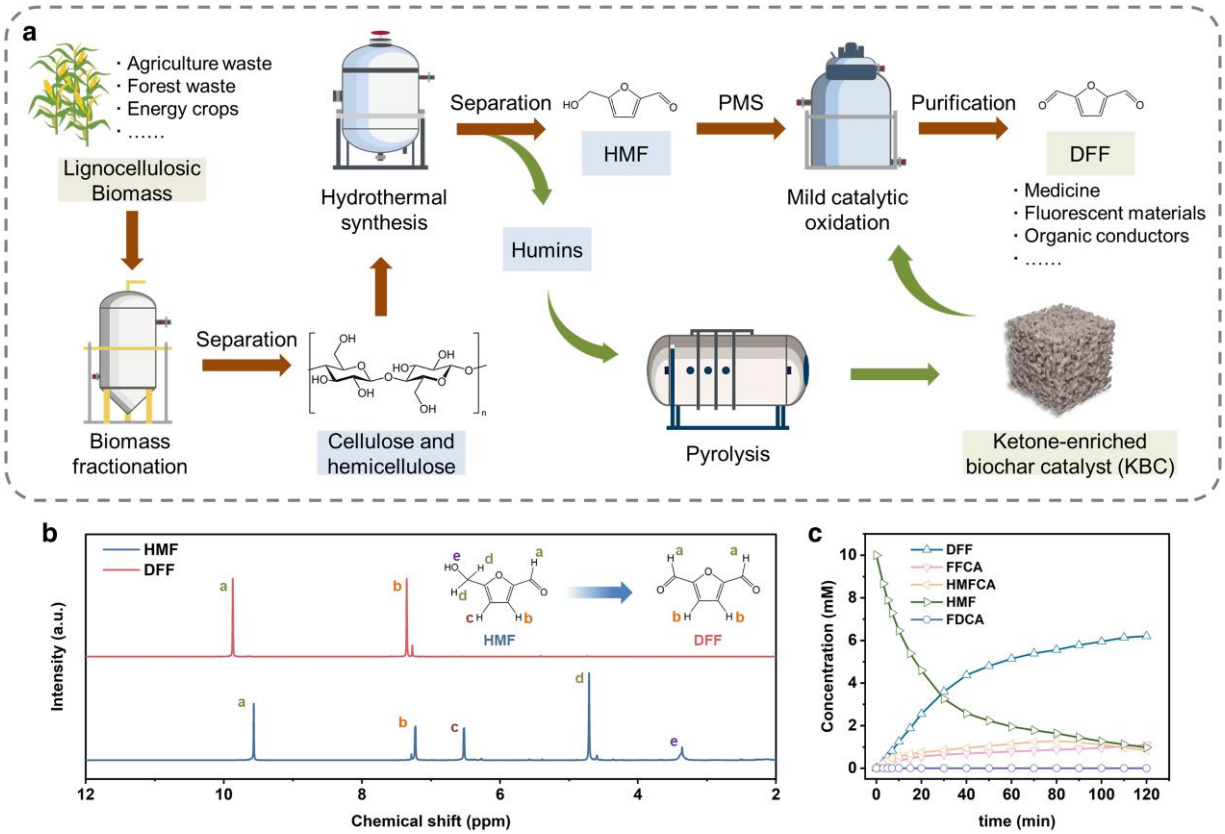

Fig. 4. Scaling up of DFF production using lignocellulosic biomass. a) Schematic illustration of an integrated process for producing DFF using lignocellulosic biomass. b) ^{1}H NMR spectra of purified HMF and DFF from straw biomass. c) Concentration versus time plot for DFF preparation using lignocellulosic biomass-derived HMF and biochar.

feasibility of the reaction (41). The data indicate that $^{1}O_2$ can overcome an energy barrier of 24.02 kJ/mol to abstract hydrogen atoms from C and O within the hydroxymethyl groups, culminating in the generation of DFF (Fig. 3h). Moreover, the significant negative values of hydrogen atom abstraction energy underscored the thermodynamic favorability of the reaction. Leveraging the collected information and proposed mechanism, various substrates containing hydroxyl groups were used as reactants under mild reaction conditions, all showing good conversion and yield (Fig. S24).

Feasibility of biomass-to-DFF production

Based on the efficacy of the validated catalytic system renowned for its remarkable selectivity in DFF production, we further propose a comprehensive process for synthesizing DFF from lignocellulosic biomass (Fig. 4a). This process encompasses four main stages: biomass fractionation, cellulose hydrolysis, catalyst fabrication, and DFF synthesis. Initially, the lignocellulosic biomass is recovered, dried, and pulverized, followed by fractionation to segregate cellulose and hemicellulose. These components are then subjected to direct dehydration under specific conditions, achieving a yield of 45.4% for HMF in the presence of $ZnCl_2$ and KCl, utilizing tetrahydrofuran and H_2O at a 6:1 mass ratio as solvents. The subsequent phase involves isolating HMF in an acidic solution through $NaHSO_3$ binding, then adjusting the pH to alkaline, and employing 2-methyltetrahydrofuran for extraction to yield HMF with a purity exceeding 95% (Fig. 4b). Concurrently, humins emerge as inevitable by-products, characterized by an elemental composition of ~50–60 wt% C, 4–5 wt% H, and 30–40 wt% O. The oxygen-rich nature of the humins renders them compelling candidates for the cost-effective synthesis of KBC. After extracting and isolating HMF, the washed by-product humins and dried $ZnCl_2$ and KCl are mixed and subjected to co-pyrolysis to obtain the KBC-2 catalyst. After rinse, the mixed salts can be collected and recycled to participate in converting biomass. Utilizing the humins-derived KBC-2 as catalyst, the selective catalytic oxidation of HMF yields a high conversion rate of 90.3% and a selectivity nearing 80.0% (Fig. 4c), underscoring the process's efficiency. For the separation of DFF from the reaction mixture, the aqueous layer is extracted with methyl isobutyl ketone (MIBK), leveraging DFF's lower polarity to achieve solubility in MIBK. Subsequent vacuum spinning to evaporate the lower-boiling-point solvent facilitates the recovery of high-purity DFF (Fig. 4b).

The proposed process for DFF production remains at the proof-of-concept stage, and identifying environmental and economic performances throughout its life cycle will inform future optimization efforts. Employing LCA enables a comprehensive evaluation of energy consumption and environmental impacts. Two contrasting routes, namely electrochemical synthesis from straw and thermochemical synthesis from corn starch (42, 43), were selected for comparison (Fig. 5a), and the defined scope is shown in Fig. 5b. The life-cycle inventories based on mass and energy balances for the three synthesis routes are listed in Table S5, with data sourced from the current synthesis route and literature. To delve deeper into the comparison of the three DFF synthesis routes, Fig. S25 illustrates the normalized relative contributions of each route. It is evident that the PMS oxidation synthesis route shows improvement trends in almost all impact categories,

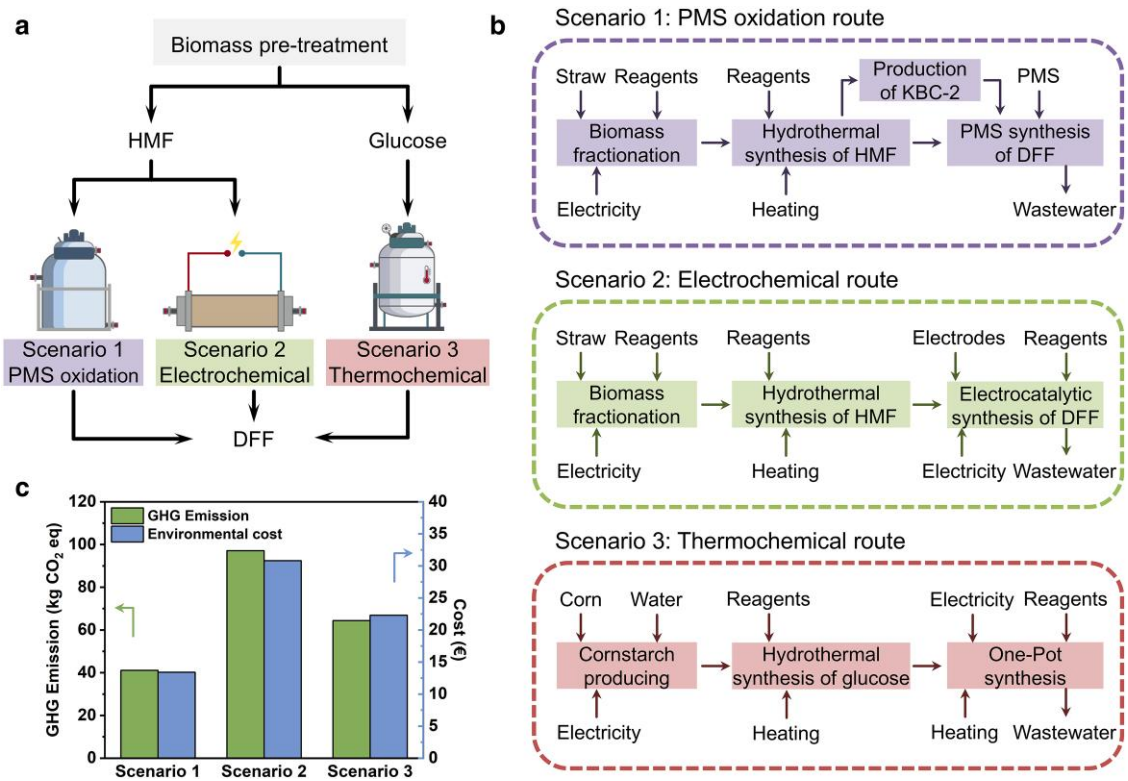

Fig. 5. Economic and sustainability analyses. a) Comparison of important aspects of the three routes for DFF production from biomass. b) System boundary of LCA for the three routes. c) Comparative life-cycle climate change impacts and the corresponding environmental cost of producing 1 kg DFF.

particularly notable in stratospheric ozone depletion, marine eutrophication, land use, and water consumption. This is attributed to the reduced use of organic reagents and energy in the synthesis process, significantly mitigating unnecessary carbon emissions and reducing environmental risks. Additionally, an assessment of the environmental footprint reveals that the proposed process has a smaller impact on global climate change compared with other synthesis routes, evidenced by lower CO_2 emissions during synthesis. The environmental cost of producing 1 kg DFF via our proposed process was estimated to be €13.4, lower than that of the electrochemical (€30.8) and thermochemical synthesis routes (€22.3) (Fig. 5c), underscoring its economic viability and efficiency.

Conclusion

In summary, we proposed a new catalytic approach for the selective oxidation of HMF to DFF by $^1O_2$ generation via the activation of PMS. Porous ketone-rich (45.5% oxygen-containing functional groups) biochar catalysts were successfully developed by a $ZnCl_2$/KCl mixed molten salt co-pyrolysis strategy. The ketone structure served as an electron donor to activate PMS, resulting in $^1O_2$ production. As a result, the selective oxidation of HMF to DFF was achieved with 82.3% selectivity and a 69.8% yield under mild conditions. Furthermore, we have established a green and sustainable process route that fully utilizes renewable biomass to produce DFF. By leveraging by-products and PMS to enhance DFF yield, we have prioritized sustainability. This approach not only reduces energy input and the need for subsequent treatment of organic reagents but also maximizes the utilization of biomass waste. This study has paved the way for the safe, economical, and sustainable production of high-value chemical products, significantly enhancing the economic benefits of biomass utilization.

Materials and methods

Catalyst preparation

To obtain the biochar catalyst, a mixture of $ZnCl_2$ and KCl (54:46, wt.%) was thoroughly blended with trehalose at a 2:1 mass ratio and then dried at 60 °C to prepare the precursor. The obtained precursor (3 g) was subsequently placed in a tube furnace and heated to 800 °C over 2 h at a heating rate of 5 °C min^{-1} under nitrogen protection. The resultant pyrolysis product underwent triple washes with 1 M HCl and ultrapure water, followed by drying at 60 °C for 12 h, yielding the catalyst designated as KBC-2. For comparative purposes, the catalysts synthesized without mixed salts and with mixed salt-to-biomass ratios of 1:1 and 3:1 were labeled BC, KBC-1, and KBC-3, respectively.

Material characterizations

SEM (Sigma 300, ZEISS Co., Germany) was used to observe the morphology and structure of the catalysts. XRD (PANalytical X'Pert3 Powder, The Netherlands) with Cu Kα radiation (λ = 1.5418 Å) and Raman spectrometry (XploRA, Horiba Co., Japan) were used to examine the crystallographic structure of the samples. XPS (K-Alpha, Thermo Scientific Inc., USA) was performed with Al Kα radiation (1,486.6 eV) to study the surface chemical species of the samples. Nitrogen adsorption–desorption curves were collected by means of a physisorption instrument (ASAP 2460, Micromeritics Co., USA). TGA and DSC analyses were performed using a synchronous thermal analyzer (TG-DSC, STA 449 F3, Netzsch Co., Germany) in the range of 40–800 °C at a heating rate of 5 °C min^{-1} under a N_2 atmosphere. The functional groups of the samples were characterized by FTIR (Thermo Nicolet iS50, USA). EPR (EPR200M, Chinainstru & Quantumtech Co., China) tests were conducted to study the generation of reactive oxygen

species during the selective oxidation of HMF. For this purpose, DMPO was employed to trap ·OH and $SO_4^{\cdot-}$, while TEMP was utilized to trap $^1O_2$.

Selective oxidation of HMF

In the process of selectively oxidizing HMF, 5 mg catalyst was dispersed in 5 mL ultrapure water containing 10 mM HMF (in borate buffer, pH =7.0). To initiate the reaction, PMS was added to the solution to achieve a concentration of 20 mM. This mixture was then stirred at 50° C and 600 rpm for a duration of 2 h. Samples were withdrawn at intervals, filtered, and analyzed using high-performance liquid chromatography (LC-16, Shimadzu Co., Japan). Detailed calculations for HMF conversion, DFF selectivity, and DFF yield are provided in the Supplementary Note.

Life-cycle assessment

The environmental impact and cost analysis for producing 1 kg of DFF were evaluated using SimaPro v.9 (PRé Consultants) software. Straw was chosen as the primary biomass resource, with both electrochemical and thermochemical processes being used as benchmark references for this assessment. Data for the analysis were collected from this study, literature, and Ecoinvent 3 database. Overall life-cycle impacts were assessed using the ReCipe 2016 v1.1 midpoint method, with monetization based on European Environmental Prices (2015).

Supplementary Material

Supplementary material is available at *PNAS Nexus* online.

Funding

The authors greatly acknowledge the financial support of the National Natural Science Foundation of China (51908172, 51821006, and 52192684).

Author Contributions

K.-Y.C., B.-C.H., and H.-Q.Y. conceived the concept and composed the manuscript. K.-Y.C., L.-Q.Y., and Y.-X.H. carried out the experiments and collected and analyzed the data. B.-C.H., R.-C.J., and H.-Q.Y. coordinated the project and analyzed the data. All of the authors provided discussion of the data and ideas and gave input on the manuscript.

Data Availability

All data are included in the article and/or Supplementary Information.

References

1 De Luna P, *et al.* 2020. What would it take for renewably powered electrosynthesis to displace petrochemical processes? *Science*. 367:eabb0992.
2 Guo L, *et al.* 2023. Advances in selective electrochemical oxidation of 5-hydroxymethylfurfural to produce high-value chemicals. *Adv Sci*. 10:2205540.
3 Corma A, Iborra S, Velty A. 2007. Chemical routes for the transformation of biomass into chemicals. *Chem Rev*. 107:2411–2502.
4 Bozell JJ. 2010. Connecting biomass and petroleum processing with a chemical bridge. *Science*. 329:522–523.
5 Ragauskas AJ, *et al.* 2006. The path forward for biofuels and biomaterials. *Science*. 311:484–489.
6 Li C, Zhao X, Wang A, Huber GW, Zhang T. 2015. Catalytic transformation of lignin for the production of chemicals and fuels. *Chem Rev*. 115:11559–11624.
7 Qi M-Y, Conte M, Anpo M, Tang Z-R, Xu Y-J. 2021. Cooperative coupling of oxidative organic synthesis and hydrogen production over semiconductor-based photocatalysts. *Chem Rev*. 121: 13051–13085.
8 Zhang Z, Huber GW. 2018. Catalytic oxidation of carbohydrates into organic acids and furan chemicals. *Chem Soc Rev*. 47: 1351–1390.
9 Lv G, *et al.* 2015. Graphene oxide: a convenient metal-free carbocatalyst for facilitating aerobic oxidation of 5-hydroxymethylfurfural into 2, 5-diformylfuran. *ACS Catal*. 5:5636–5646.
10 Han G, *et al.* 2017. Visible-light-driven valorization of biomass intermediates integrated with H_2 production catalyzed by ultrathin Ni/CdS nanosheets. *J Am Chem Soc*. 139:15584–15587.
11 Zhang Z, Deng K. 2015. Recent advances in the catalytic synthesis of 2,5-furandicarboxylic acid and its derivatives. *ACS Catal*. 5: 6529–6544.
12 You B, Jiang N, Liu X, Sun Y. 2016. Simultaneous H_2 generation and biomass upgrading in water by an efficient noble-metal-free bifunctional electrocatalyst. *Angew Chem Int Ed*. 55:9913–9917.
13 Zhang L-X, Tang Z-R, Qi M-Y, Xu Y-J. 2024. Engineering semiconductor quantum dots for co-upcycling of CO_2 and biomass-derived alcohol. *J Mater Chem A*. 12:19029–19038.
14 Xia T, *et al.* 2022. Sunlight-driven highly selective catalytic oxidation of 5-hydroxymethylfurfural towards tunable products. *Angew Chem Int Ed*. 61:e202204225.
15 Cleveland JL, Kastan MB. 2000. A radical approach to treatment. *Nature*. 407:309–311.
16 Di Mascio P, *et al.* 2019. Singlet molecular oxygen reactions with nucleic acids, lipids, and proteins. *Chem Rev*. 119:2043–2086.
17 Yang Z, Qian J, Yu A, Pan B. 2019. Singlet oxygen mediated iron-based Fenton-like catalysis under nanoconfinement. *Proc Natl Acad Sci U S A*. 116:6659–6664.
18 Montgomery RE. 1974. Catalysis of peroxymonosulfate reactions by ketones. *J Am Chem Soc*. 96:7820–7821.
19 Hussain H, Green IR, Ahmed I. 2013. Journey describing applications of oxone in synthetic chemistry. *Chem Rev*. 113:3329–3371.
20 Li J, *et al.* 2017. Improving the alkene selectivity of nanocarbon-catalyzed oxidative dehydrogenation of *n*-butane by refinement of oxygen species. *ACS Catal*. 7:7305–7311.
21 Yu Z, *et al.* 2016. Polymerization under hypersaline conditions: a robust route to phenolic polymer-derived carbon aerogels. *Angew Chem Int Ed*. 55:14623–14627.
22 Wu Z-Y, *et al.* 2018. Transition metal-assisted carbonization of small organic molecules toward functional carbon materials. *Sci Adv*. 4:eaat0788.
23 Wang C, *et al.* 2018. A green and scalable route to yield porous carbon sheets from biomass for supercapacitors with high capacity. *J Mater Chem A*. 6:1244–1254.
24 Ma Z, *et al.* 2014. Highly mesoporous carbons derived from biomass feedstocks templated with eutectic salt $ZnCl_2$/KCl. *J Mater Chem A*. 2:19324–19329.
25 Nie J, Xie J, Liu H. 2013. Efficient aerobic oxidation of 5-hydroxymethylfurfural to 2,5-diformylfuran on supported Ru catalysts. *J Catal*. 301:83–91.
26 Buxton GV, Greenstock CL, Helman WP, Ross AB. 1988. Critical review of rate constants for reactions of hydrated electrons, hydrogen atoms and hydroxyl radicals (·OH/·O$^-$) in aqueous solution. *J Phys Chem Ref Data*. 17:513–886.

27 Anipsitakis GP, Dionysiou DD. 2004. Radical generation by the interaction of transition metals with common oxidants. *Environ Sci Technol*. 38:3705–3712.
28 Yun E-T, Lee JH, Kim J, Park H-D, Lee J. 2018. Identifying the nonradical mechanism in the peroxymonosulfate activation process: singlet oxygenation versus mediated electron transfer. *Environ Sci Technol*. 52:7032–7042.
29 Huang Z, Bao H, Yao Y, Lu W, Chen W. 2014. Novel green activation processes and mechanism of peroxymonosulfate based on supported cobalt phthalocyanine catalyst. *Appl Catal B*. 154–155:36–43.
30 Li H-R, Wu L-Z, Tung C-H. 2000. Reactions of singlet oxygen with olefins and sterically hindered amine in mixed surfactant vesicles. *J Am Chem Soc*. 122:2446–2451.
31 Ren W, *et al*. 2020. The intrinsic nature of persulfate activation and N-doping in carbocatalysis. *Environ Sci Technol*. 54:6438–6447.
32 Ren W, *et al*. 2019. Activation of peroxydisulfate on carbon nanotubes: electron-transfer mechanism. *Environ Sci Technol*. 53:14595–14603.
33 Huang Y, Hu H. 2020. The interaction of perrhenate and acidic/basic oxygen-containing groups on biochar surface: a DFT study. *Chem Eng J*. 381:122647.
34 Qi W, *et al*. 2013. Oxidative dehydrogenation on nanocarbon: identification and quantification of active sites by chemical titration. *Angew Chem Int Ed*. 52:14224–14228.
35 Verstraeten SV, Lucangioli S, Galleano M. 2009. ESR characterization of thallium(III)-mediated nitrones oxidation. *Inorg Chim Acta*. 362:2305–2310.
36 Zhang L, *et al*. 2021. Carbon nitride supported high-loading Fe single-atom catalyst for activation of peroxymonosulfate to generate $^1O_2$ with 100% selectivity. *Angew Chem Int Ed*. 60:21751–21755.
37 Li J, *et al*. 2020. Understanding of the oxidation behavior of benzyl alcohol by peroxymonosulfate via carbon nanotubes activation. *ACS Catal*. 10:3516–3525.
38 Yang P, *et al*. 2023. Regulating the local electronic structure of copper single atoms with unsaturated B,O-coordination for selective $^1O_2$ generation. *ACS Catal*. 13:12414–12424.
39 Sousa SF, Fernandes PA, Ramos MJ. 2007. General performance of density functionals. *J Phys Chem A*. 111:10439–10452.
40 Reed AE, Curtiss LA, Weinhold F. 1988. Intermolecular interactions from a natural bond orbital, donor-acceptor viewpoint. *Chem Rev*. 88:899–926.
41 Armaković S, Armaković SJ. 2023. Atomistica.online—web application for generating input files for ORCA molecular modelling package made with the Anvil platform. *Mol Simulat*. 49:117–123.
42 Nguyen QNB, *et al*. 2022. Direct and low-cost transformation of glucose to 2,5-diformylfuran by $AlCl_3{\cdot}6H_2O$, sulfur, and dimethyl sulfoxide. *Mol Cat*. 530:112588.
43 Kisszekelyi P, *et al*. 2020. Selective electrocatalytic oxidation of biomass-derived 5-hydroxymethylfurfural to 2,5-diformylfuran: from mechanistic investigations to catalyst recovery. *ChemSusChem*. 13:3127–3136.